LRP 554/96 September 1996

VOLTAGE UNIFORMITY STUDY IN LARGE-AREA REACTORS FOR RF PLASMA DEPOSITION

L. Sansonnens, A. Pletzer, D. Magni,
A.A. Howling, Ch. Hollenstein &
J.P.M. Schmitt

submitted for publication to
Plasma Sources Science and Technology

Voltage uniformity study in large-area reactors for RF plasma deposition

L Sansonnens, A Pletzer†, D Magni, A A Howling, Ch Hollenstein, and J P M Schmitt‡

Centre de Recherches en Physique des Plasmas
Ecole Polytechnique Fédérale de Lausanne
PPH - Ecublens, CH-1015 Lausanne, Switzerland
sansonnens@crpp.epfl.ch
†Association Euratom - Confédération Suisse
‡Balzers Process Systems, 5 Rue Léon Blum, F-91120 Palaiseau, France

Abstract.

Non-uniform voltage distribution across the electrode area results in inhomogeneous thin-film RF plasma deposition in large area reactors. In this work, a two-dimensional analytic model for the calculation of the voltage distribution across the electrode area is presented. The results of this model are in good agreement with measurements performed without plasma at 13.56 MHz and 70 MHz in a large area reactor. The principal voltage inhomogeneities are caused by logarithmic singularities in the vicinity of RF connections and not by standing waves. These singularities are only described by a two-dimensional model and cannot be intuitively predicted by analogy to a one-dimensional case. Plasma light emission measurements and thickness homogeneity studies of a-Si:H deposited films show that the plasma reproduces these voltage inhomogeneities. Improvement of the voltage uniformity is investigated by changing the number and position of the RF connections.

PACS numbers: 52.75.Rx 81.15.Gh

1. Introduction

Plasma enhanced chemical vapour deposition (PECVD) of thin films such as amorphous silicon or silicon oxide has widespread applications, especially in the field of photovoltaic solar cells and thin film transistors for flat screen production. Industrial applications require high deposition rates over large areas (35 cm $\times$ 45 cm or more for flat screen applications) and a uniformity in layer thickness to better than $\pm$ 5% for flat screens and about $\pm$ 10% for solar cells.

The most commonly-used deposition technique uses a parallel plate reactor with 13.56 MHz excitation frequency. The choice of this frequency is dictated by convention and the consequent availability of RF technology suited to this frequency, rather than by optimization of the physical processes in the discharge. There exists, however, a growing body of experimental [1, 2, 3, 4, 5, 6, 7, 8] and modelling [9, 3, 10, 5] evidence to show that VHF (Very High Frequency: 30-300 MHz) excitation can be used to advantage, primarily to obtain good quality films at high deposition rates. Generally, these high frequency studies are made in small reactors and they need to be upscaled in order to meet the large area requirement for industrial applications.

Schmitt [11, 12] has pointed out that inhomogeneity problems could occur in the electrode voltage distribution when the electrode dimensions become comparable to a quarter of the free-space wavelength associated with the excitation frequency ($\lambda/4$ is 5.53 m at 13.56 MHz but only 0.75 m at 100 MHz), by analogy to the standing wave on a one-dimensional transmission line. Kuske et al [13] proposed some possible solutions to improve the voltage homogeneity by modifying the power feeding of the electrode or by terminating the electrode edge with additional inductances. The problem of voltage distribution across the electrode surface becomes important if the RF frequency is increased for a fixed reactor size, or at the standard 13.56 MHz frequency for larger reactors.

The one-dimensional transmission line description gives a first insight into the inhomogeneity problem, but the study of a plasma reactor with one or more RF connections needs at least a two-dimensional model for a quantitative evaluation. In fact, as the frequency is increased, the inhomogeneity is principally due to a singularity associated with the local current source, before standing wave effects become important. This singularity is only described by a two-dimensional model and cannot be intuitively predicted by analogy to a one-dimensional case. The calculation of the voltage distribution in a RF plasma reactor is analogous to the design of microstrip devices [14, 15] which use millimetric structures at GHz frequencies.

In this paper we show measurements of the voltage uniformity, in the absence of plasma, across a large area rectangular plasma reactor (57 cm $\times$ 47 cm) with RF and ground connections located on the edge of the RF electrode and reactor wall respectively

for 13.56 MHz and 70 MHz excitation frequencies. An analytic solution for the voltage distribution across the electrodes satisfying a two-dimensional Helmholtz equation, based on the Green function technique is presented in § 3. Experiments and calculations are in good agreement, both exhibiting a voltage drop in the vicinity of the source associated with the logarithmic singularity of the two-dimensional Green's function which is particularly noticeable at high frequencies. Furthermore, measurements of the plasma light emission intensity across the electrode and of the thickness uniformity of a-Si:H films deposited on 35 cm × 45 cm glass substrates show that the presence of the plasma does not short-circuit the voltage inhomogeneity.

In § 4.2 and in § 4.3, we investigate the effect of modifications to the number and position of RF and ground connections to improve the homogeneity. The electrode voltage and deposition uniformity were first increased by introducing four corner RF connections in place of one, but in § 4.3, we show that better uniformity is obtained when the RF and ground connections are centred on the top of the RF electrode and reactor cover respectively. Finally, we summarize the results obtained for the different cases and evaluate the frequency limits in the light of industrial homogeneity requirements.

We concentrate here on the voltage distribution across the electrode as the cause of inhomogeneity. However, it is important to note that, for example, powder contamination of the plasma [16] or gas depletion [11, 12] can also produce significant inhomogeneity. Nevertheless, in all cases any voltage inhomogeneity must be avoided for uniform deposition in large areas or at high RF frequencies.

2. Experimental setup

The plasma reactor investigated of figure 1 is a modified version of the industrial KAI type reactor commercialized by Balzers SA for thin film deposition. It consists of a rectangular plasma reactor 57 cm long by 47 cm wide installed inside a larger vacuum chamber. A RF rectangular electrode (56.2 cm × 46.2 cm and 0.7 cm thick) is suspended 25 mm above the reactor floor, and the space between the top of the RF electrode and the reactor cover is 6 mm. In this basic version, the ground return is connected to the reactor wall midway on the longer side, while the RF connection is located on the top of the RF electrode at 2 cm from the corresponding edge [see figure 1(b)]. The RF power is capacitively coupled to the RF electrode via a matching network at the input of which the forward and reflected RF power are measured with a directional power meter. The process gases are introduced through a showerhead incorporated in the RF electrode and residual gases are pumped out through the back wall designed as a coarse grid. The glass substrate used for a-Si:H deposition here was 35 cm × 45 cm and 1 mm thick, centrally placed on the reactor floor (grounded electrode). For high quality film deposition, the reactor was uniformly heated to 200 °C.

The interelectrode voltage distribution across the electrode surface in the plasma zone was measured in the absence of plasma with a passive RF voltage probe (Philips PM 8932) connected to an oscilloscope which was floating for RF measurements. The probe RF tip contacted the RF electrode at one point, and the probe ground tip contacted the corresponding opposite point of the ground electrode as shown in figure 1(a). The interelectrode voltage distribution was obtained by moving both probe contacts across the electrode area.

Large windows were introduced into our laboratory version of the industrial reactor to permit optical measurements (figure 1(b)). In particular, the front door was replaced by a full width window which permitted a complete cross-sectional view of the plasma. All windows were positioned at the end of 10 cm long extension tubes to prevent problems of deposition. Grids placed at the reactor wall preserved electrical continuity and plasma confinement. A charge-coupled device (CCD) camera was used to monitor a two-dimensional image of the plasma light emission where each pixel represents the line-integrated intensity emitted along the viewing axis.

The global uniformity of the deposited film was measured by an ex-situ interferometry technique [17, 16]: The substrate was illuminated with a homogeneous white light source, and the spatial thin film interference fringes were obtained by monitoring the transmitted light through a 707 nm interference filter with a CCD camera. Neighbouring light and dark regions (half of an interference fringe) correspond to a 44 nm difference in film thickness, taking the a-Si:H refractive index to be 4 [18]. The direction of the film thickness gradient, which is not given by this global technique, was determined by means of a second ex-situ interferometer system [16]: The transmitted white light was collected at a point with an optical fibre and analyzed by a monochromator and optical multichannel analyzer. If the detection point was then moved across a region where the film becomes thicker, the interference extrema were displaced towards smaller wavelengths.

3. Theoretical model

3.1. Green's function solutions

Rather than tacking our problem in the full geometrical complexity of figure 1, let us first consider the problem of solving Maxwell's equations for a system composed of two equal-sized, lossless, metallic plates which are positioned along the (x, y) planes at $z = \pm d/2$. Because of the planar geometry and since the inter-electrode distance d is assumed small compared to the x and y sizes, the electric field $\mathbf{E} = \mathbf{E_z(x,y)}\hat{\mathbf{z}}$ can be taken to be perpendicular to the electrodes (no fringing effect) with E_z constant along the z direction (homogeneous interstitial medium). Assuming furthermore a $\exp(-i\omega t)$ time dependence, it can easily be shown [15] that Maxwell's equations then reduce to a

driven, two-dimensional Helmholtz equation

$$\left(\nabla^2 + k^2\right) V(\boldsymbol{x}) = i\omega\mu d J_z(\boldsymbol{x}), \qquad \boldsymbol{x} = (x, y) \in \Omega \tag{1}$$

for the voltage $V \equiv -\int dz E_z = -E_z d$ between plates, where $\nabla^2 \equiv \partial^2/\partial x^2 + \partial^2/\partial y^2$ and,

$$k^2 \equiv \epsilon\mu\omega^2 \qquad \left(= \frac{\omega^2}{c^2} \text{ in vacuum}\right), \tag{2}$$

ϵ and μ being the permittivity and permeability, respectively, of the interstitial medium. The driving term in (1) is proportional to the current density J_z oscillating at angular frequency ω. For simplicity, it is convenient to assume the source to be applied symmetrically on both plates $J_z(z = -d/2) = -J_z(z = d/2)$, though the generalization to asymmetric sources is straightforward. In the latter case, J_z should be regarded as the sum of the RF and ground electrodes current densities with a negative sign associated to the bottom (ground) excitation. We shall discuss for convenience only the voltage distribution occurring on the top electrode (RF), keeping in mind that there exists this duality between RF and ground electrodes.

Equation (1) can be solved using the Green function method [19]. Let the Green function $g(\boldsymbol{x}; \boldsymbol{x}_s)$ satisfying appropriate, homogeneous boundary conditions be a solution of the Helmholtz equation driven by a Dirac source at xv_s:

$$\left(\nabla^2 + k^2\right) g(\boldsymbol{x}; \boldsymbol{x}_s) = \delta(\boldsymbol{x} - \boldsymbol{x}_s) \qquad \boldsymbol{x}_s \in \Omega. \tag{3}$$

Then, by virtue of the superposition principle, the total solution

$$V(\boldsymbol{x}) = \int d\Omega_s g(\boldsymbol{x}; \boldsymbol{x}_s) s(\boldsymbol{x}_s) \tag{4}$$

can be written as the sum of all responses to Dirac sources, weighted by the source distribution function $s \equiv i\omega\mu d J_z$.

The Green function is generally not known, except in the case of boundaries at infinity [19]. The asymptotic behaviour of the Green function near the δ source is, however, well known from standard textbooks on differential equations. It can easily be obtained by surface integration of (3) over a circular area of radius R about the Dirac source point. Since the Dirac source strongly affects the voltage gradient in the vicinity of $\boldsymbol{x}_s$, the term proportional to k^2 in (3) can be neglected provided R remains small. From the divergence theorem one then gets $\partial g(\boldsymbol{x}, \boldsymbol{x}_s)/\partial R \approx 1/(2\pi R)$ or

$$g(\boldsymbol{x}, \boldsymbol{x}_s) \to \frac{1}{2\pi} \ln(R/R_0); \qquad R \equiv |\boldsymbol{x} - \boldsymbol{x}_s| \tag{5}$$

as $R \to 0$, where R_0 is a constant of integration. Thus, a point-like connection produces a logarithmic voltage singularity in two dimensions. A similar calculation in one dimension would show that the voltage remains bounded although the derivative is discontinuous at

the source point. This emphasizes the importance of a full two-dimensional description. Property (5) is essential to understand the experimental and analytic results shown in § 4.

A closed form of the Green function can be obtained for simple geometries, i.e. when arbitrary functions can be expanded

$$f(\boldsymbol{x}) = \sum_n f_n \Phi_n(\boldsymbol{x}) \tag{6}$$

in a complete set of eigenfunctions $\Phi_n(\boldsymbol{x})$,

$$\left(\nabla^2 + k^2\right) \Phi_n(\boldsymbol{x}) = \lambda_n \Phi_n(\boldsymbol{x}), \tag{7}$$

satisfying appropriate, homogeneous boundary conditions. The Green function then reads [14, 15]

$$g(\boldsymbol{x}; \boldsymbol{x}_s) = \sum_n \frac{\Phi_n(\boldsymbol{x})\Phi_n(\boldsymbol{x}_s)}{\lambda_n \langle \Phi_n, \Phi_n \rangle}, \qquad \langle \Phi_n, \Phi_n \rangle \equiv \int d\Omega {\Phi_n}^2. \tag{8}$$

3.2. Boundary conditions and impedance discontinuity

At the frequencies of interest, the skin current effect (skin depth = 22 μm at 13.56 MHz for aluminium) prevents us from regarding the electrodes as homogeneous, plane conducting plates so that the model described above cannot be applied without special care. Instead, the RF electrode appears as the juxtaposition of two thin current layers (at the top and bottom) which connect at the edges (figure 2(a)). Since the current layer thickness is small compared to the plate size so that the two-dimensional approximation remains valid, it is convenient to "unfold" the RF electrode so as to form a periodic lattice, as shown in figure 2(b). For instance, the current leaving the right-hand edge of the bottom layer reappears at the left-hand side of the top layer, and so on. The size of equivalent RF electrode is now $2L_x \times 2L_y$ with $V(\boldsymbol{x})$ satisfying periodic boundary conditions, and a source S = (x_s, y_s) positioned on the top of the RF electrode is modeled in this equivalent geometry by two sources $S_1 = (x_s, -y_s)$ and $S_2 = (-x_s, y_s)$. The periodic bondaries allow us to focus on the elementary cell of figure 2(b) only. The eigenfunctions of (7) and (8) are therefore

$$\Phi_{\boldsymbol{n}} = \frac{\exp(i\pi(n_x x/L_x + n_y y/L_y))}{2\sqrt{L_x L_y}} \tag{9}$$

where $\boldsymbol{n} = \{n_x, n_y\}$, with $< \Phi_{\boldsymbol{n}}, \Phi_{\boldsymbol{n}'} >= \delta_{\boldsymbol{n},\boldsymbol{n}'}$ and $\lambda_{\boldsymbol{n}} = k^2 - \pi^2 {n_x}^2/L_x^2 - \pi^2 {n_y}^2/L_y^2$.

There is yet another complication to take into account, namely the fact that the distance d separating the RF electrode from the ground electrode is different on the top and bottom. The characteristic impedance Z scaling as $\sim d$, the requirements of continuous voltage and current (or electric and magnetic fields)

$$V|_b \quad = V|_t$$

$$\left.\frac{1}{Z_b}\frac{\partial V}{\partial n}\right|_b = \left.\frac{1}{Z_t}\frac{\partial V}{\partial n}\right|_t \tag{10}$$

across the bottom-top interface, can generally only be achieved with a discontinuous normal derivative $\partial V/\partial n$ at the interfaces (edges). There is however a simple way to construct by linear combination, a $V(\boldsymbol{x})$ solution which: (a) satisfies (1), (b) has period boundary conditions and (c) possesses the derivative discontinuity according to (10). To be more specific, let us assume, as it is the case in the experimental set-up, that the RF connection is modelled by a δ function that is located on the top layer. The source will radiate $\Phi_{\boldsymbol{n}}$ waves but some will bounce back due to reflections occurring at the interface. For an observer on the top layer, there is no way to discriminate between reflected waves and those emitted by a mirror source on the bottom layer (analogous the image method in electrostatics, see figure 3). It is not difficult to prove that the amplitude of the image source must be $(Z_b - Z_t)/(Z_b + Z_t)$, that is exactly the reflection coefficient. In the case where the top and bottom sizes are identical, one can verify that reflections at the boundaries of the elementary cell do not introduce additional image sources. In the limit of $Z_b \to 0$, the image source has the same but opposite amplitude whereas the image source amplitude is equal to the source amplitude in the $Z_b \to \infty$ limit. Homogeneous Dirichlet boundary conditions apply at the top edge in the former case whereas homogeneous Neumann boundary conditions apply in the second one.

A solution on the bottom side can then be constructed by multiplying the source by the transmission coefficient $2Z_b/(Z_b + Z_t)$. Hence, the impedance discontinuity will not affect the behaviour of the solution on the bottom layer, merely introducing a multiplicative coefficient. This in contrast to the top layer where the source is located and where the behaviour of V is modified by reflections.

3.3. Standing wave and finite area connector

We are now able to identify two distinct regimes of voltage inhomogeneity. First, the regime where inhomogeneity is dominated by the logarithmic singularity (5) of a point-like connection. A large number of Fourier components are required to correctly represent this singularity. Clearly this regime can only take place off resonance. Second, the standing wave regime obtained when $\lambda_{\boldsymbol{n}} = 0$ in (8) and only one Fourier mode survives. The voltage inhomogeneity then results from the difference of amplitude between an antinode and a node through the parameter k. Since we allow n_x and n_y to vary from 0, 1, 2 $\cdots$, the lowest resonance is at $k^2 = 0$, yielding a flat voltage distribution.

These two regimes are best illustrated in figure 4 for two types of sources: an edge line source $s = \delta(x)$ ((a) and (b)) and an edge point source $s = \delta(x)\delta(y - L_y/2)$ ((c) and (d)), at two frequencies f = 150 MHz (left) and 300 MHz (right). In figure 4(a)

we have chosen the wavelength $\lambda \approx L_x/4$, the problem becomes one dimensional in this case due to the choice of the line source with the voltage remaining bounded in contrast to case (c) where the source is peaked. The main source of voltage inhomogeneity at $f = 150$ MHz for a point-like source is due to the logarithmic singularity [case (c)]. As the frequency increases to $f = 300$ MHz we approach the $(n_x = 1, n_y = 0)$ resonance. The one-dimensional (b) and two-dimensional (d) cases are qualitatively similar because of the negligible role played by the source. The singular source effects reappear at higher frequencies but their coupling to resonant, standing wave inhomogeneities becomes more effective due to the higher density of resonances in this part of the spectrum (results not shown).

It may be appropriate to comment at this point on the finite size effect of a source. If we replace the δ function by a source which is zero everywhere except on a area πa^2 where its amplitude is constant and inversely proportional to the area [a crude approximation of $\delta(\boldsymbol{x})$], one then recovers the logarithmic function (5) outside the radius a, whereas $\partial g(\boldsymbol{x}, \boldsymbol{x}_s)/\partial R \approx R/(2\pi a^2)$ inside it. The replacement of a finite-sized source by a Dirac function in the simulations is therefore valid outside the contact area.

4. Results

4.1. Electrode with a single edge connection

Figure 5 shows the measured and calculated RF voltage amplitude distributions across the electrode for two frequencies. The measurements were performed without plasma as described in § 2, and the calculations were made with the model developed in § 3.1. The RF and ground return connections were located midway along the long edge of the RF electrode and ground reactor wall respectively as described in § 2. This position is indicated by the black point on the figure axis.

At 13.56 MHz, the measured voltage amplitude is almost constant across the whole electrode area, whereas at 70 MHz, it is highly non-uniform in the vicinity of the RF connection. This observed non-uniformity is well described by the logarithmic singularity due to a local source as predicted in the two-dimensional model and cannot be described by an one-dimensional model. The voltage inhomogeneity Δ_v can be defined by the expression:

$$\pm\Delta_v \equiv \frac{V_{max} - V_{min}}{V_{max} + V_{min}} \tag{11}$$

where V_{max} and V_{min} are respectively the maximum and minimum peak-to-peak voltages measured over the electrode area. Although (11) is experimentally convenient, we are conscious that this expression becomes formally one for a point-like connector due to the singularity of the voltage but in reality, the finite contact area of the RF connector smears out the singularity. We find $\Delta_v = \pm\ 0.5\%$ at 13.56 MHz while $\Delta_v = \pm\ 30\%$ at

70 MHz. These results show that an increase in the RF frequency strongly increases the voltage inhomogeneity across the electrode.

The form of the calculated voltage distribution is in good agreement with the experiments, although the calculated voltage minimum is more pronounced than in the measurements. This is due to the fact that the true RF contact point was 3 cm wide whereas the source was taken to be point-like in the calculations. The choice of a Dirac source is justified by the fact that the finite contact size only affects the voltage inside the contact area, as discussed in § 3.3. Taking this into account, it is preferable, for a quantitative comparison of calculations and measurements, to use a point located not too close to the RF connection; the corner of the electrode located on the side of the RF connection is a suitable choice. At 70 MHz the voltage amplitude on this corner is about 85% of the maximum voltage and the calculated one is 88%. At 13.56 MHz both measured and calculated values exceed 99.5%. The small discrepancy between the measured and calculated values at 70 MHz could be caused by the effect of the reactor walls which increase the effective ground electrode area. In the analytical model, these walls would transform the two-dimensional calculation into a three-dimensional problem. We conclude that the two-dimensional analytical solution gives not only a good qualitative solution for the form of the voltage distribution, but also, with the precaution discussed above, a good quantitative approximation to the measurements.

The persistence of non-uniformity in the presence of plasma is demonstrated in figures 6 and 7. Figure 6 shows the emission intensity across the electrode width of an argon plasma for three excitation frequencies. These intensity profiles were recorded with the CCD camera as described in section § 2. The position of the RF connection is on the left side. The intensity on this side of the reactor decreases as the RF frequency increases, which is a direct consequence of the voltage diminution near the RF connection when the RF frequency increases. At low RF power and high frequency (above 40 MHz), a plasma exists only in the right hand side of the reactor, opposite the RF connection. In this case the voltage on the left side of the reactor is not sufficient to sustain the plasma. A quantitative comparison between the emission profile and the voltage distribution in vacuum would be complicated because the light is line-integrated along the viewing axis and also, the plasma emission distribution is not simply related to the electrode voltage.

The fact that the plasma is not able to short circuit the voltage inhomogeneity is not trivial. The plasma bulk is a good conducting medium and we can suppose that there is no lateral potential gradient in the plasma. In fact, all the voltage inhomogeneity must occur across the plasma sheaths which can be considered as approximately capacitive. The bulk plasma would therefore be equipotential, but bounded by sheaths across which the RF voltage amplitude varies with position over the reactor surface. In this way, the power dissipated in the plasma can be spatially inhomogeneous without the existence of large circulating currents. A decrease in the plasma sheath voltage would affect the

electron heating and so decrease the plasma emission. The understanding of such an inhomogeneous plasma needs further investigation and could be an interesting subject for plasma simulation studies.

The thin film interferograms in figure 7 show the global uniformity for two a-Si:H films deposited at 13.56 MHz and 70 MHz. The plasma conditions were chosen to limit the formation of powder, because powder distribution in the plasma strongly affects the plasma behavior and consequently the film homogeneity independently of the voltage effect [16]. In the 70 MHz case, the plasma was not completely powder free: a small amount of powder at the side of the reactor opposite the RF connection was responsible for two or three narrow interference fringes on the right edge of the film, but they have no influence on the rest of the inhomogeneity observed. The film deposited at 13.56 MHz is very uniform ($\Delta_T = \pm 1.5\%$, where Δ_T is the thickness inhomogeneity defined similarly as Δ_v in (11)), while the film deposited at 70 MHz is strongly inhomogeneous ($\Delta_T = \pm 38\%$) towards the RF connection. If we compare the form of this inhomogeneity with the voltage distribution across the electrode (figure 5), we can conclude that the voltage distribution is the source of this inhomogeneity. This is an additional demonstration that the plasma is strongly affected by the voltage distribution.

The inhomogeneity in the 70 MHz deposited film indicates that the diffusion path of the reactive species must be short (< 3 cm) since a long diffusion path would tend to average out the deposition rate across the substrate area. This point is also confirmed by the fact that no deposition is observed on the windows located at the end of the extension tubes (figure 1).

Figure 8 shows an approximate linear relation between the film thickness and the square of the voltage measured without plasma at the same point for the 70 MHz case. The thickness data were taken from figure 7(b) and the voltage data from figure 5(a). For a silane plasma without powder, a linear relation is generally observed between the square of the peak-to-peak voltage measured during the plasma and the input power into the reactor [20]. Assuming that the plasma does not affect the form of the voltage distribution across the electrode, figure 8 therefore indicates that the local deposition rate is roughly proportional to the local dissipated power.

4.2. Multi-source case

The results and calculations presented in the preceding section show that a single RF connection at the electrode edge does not satisfy the homogeneity requirement for industrial applications when operating in the VHF range. A similar limitation would also be found at 13.56 MHz if the size of the electrode were increased. A possible way to improve the uniformity, as also shown by Kuske et al. [13], is to increase the number of RF power connections. Figure 9 shows such a modification applied to our reactor: The

single RF connection is replaced by four connections located near the corners on the top of the RF electrode, while the ground return connection remains located midway on the longer side wall of the reactor. These RF and ground connection positions were not the result of an study but rather of the practical restrictions imposed by the electrode design.

Figure 10 shows the measurement and the calculation of the interelectrode voltage distribution across this modified electrode for 70 MHz frequency. The amplitudes of the RF current sources are each a quarter of the amplitude of the ground return current to conserve the total current. The measurements show that the inhomogeneity is partially distributed near to the four RF connections but the majority of the inhomogeneity remains centred near the ground connection. Clearly, the ground connection geometry in the radio-frequency domain is as important as for the RF connection. The voltage inhomogeneity obtained with this modified electrode at 70 MHz is $\Delta_v = \pm 14\%$ compared to $\Delta_v = \pm 30\%$ obtained with the single edge source configuration (compare figures 5 and 10). The voltage calculated with the analytic model is also in good agreement with the measurements for the multi-source case. We conclude that the model is not only valid for the single source case but can also be used to predict the homogeneity for more complex configurations.

Figure 11 shows the uniformity of an a-Si:H film deposited at 70 MHz with the modified electrode. As for the single source case [figure 7(b)], the inhomogeneity of the film thickness is similar in form to that of the voltage distribution. The film inhomogeneity in this case is about $\pm 18\%$, compared to the $\pm 38\%$ with the single source case; the four RF connections improved the homogeneity by a factor two. The majority of the inhomogeneity is caused by the return ground connection. Using the analytic model, we show below (in figure 13 that if four ground connections were used as for the RF connections, this inhomogeneity would be further reduced.

4.3. Electrode with a single centred connection

The results obtained in § 4.1 and in § 4.2 have shown that the majority of the voltage distribution inhomogeneity is located in the vicinity of the connections. When the connections are located on the edge of the reactor, this drastically decrease the film thickness homogeneity. In § 4.2, a better homogeneity was obtained by increasing the number of RF connections on the edge of the RF electrode. Another way to increase the homogeneity is to move the RF and ground connections to the centre of the top of the RF electrode and of the reactor cover respectively. Due to the skin effect of the current propagation, this configuration maximises the distance between the source and the plasma zone. Figure 12 shows the measured and the calculated voltage distribution across the electrode obtained in this configuration for 70 MHz frequency. As expected,

the singularity associated with the source does not affect the voltage in the plasma zone, and the voltage inhomogeneity obtained in this case is $\Delta_v = \pm 3\%$. The good correspondence between measurements and calculations in this case shows the ability of the model to describe configurations with connections not only located on the edge of the reactor or RF electrode.

5. Discussion and conclusions

Figure 13 presents the voltage and the film thickness inhomogeneity across the substrate area (35 cm $\times$ 45 cm) for four different connection geometries. The thickness inhomogeneity is calculated from the voltage distribution by using the linear relation between the square of the potential and the deposition rate from figure 8. It is clear that the thickness inhomogeneity predicted here is only valid for plasma conditions where this linear relation is verified; other conditions such as plasma with powder contamination could strongly degrade the expected homogeneity [16].

The close agreement between experiment and calculation shows that the model can be used to predict and optimize the RF and ground connection scheme. It appears that VHF operation in the actual modified electrode (case ii)) is limited to 55 MHz for the solar cell homogeneity requirement ($\pm$ 10%) and to 40 MHz for the flat panel display requirement ($\pm$ 5%). This limit would be raised to 80 MHz for solar cells and 60 MHz for flat panels if the ground connection was also divided into four connections (case iii)). However better results are expected for a single RF and ground connection centred on the top of RF electrode and reactor cover; the estimated limitation would be 85 MHz for flat panels and more than 100 MHz for solar cells. In all cases, 13.56 MHz operation is sufficiently homogeneous for flat panel applications.

Since the advantages of VHF operation have been demonstrated in small area reactors [1], upscaling to large surfaces must be done by taking special care over the design of the RF and ground connections to achieve the homogeneity required for industrial applications. Finally, we note the potential for specially-designed profiles of the film thickness by controlling the plasma power deposition uniformity via the RF frequency and connection geometry. In all cases, prediction for the design of a reactor could be made by using the two-dimensional model presented in this paper.

Acknowledgments

We thank the IMT Neuchâtel group of Professor Shah for useful discussions and encouragement, and L Gabella and J Redondo for assistance in computer modelling. This work was funded by Swiss Federal Research Grant BEW 9400051 and partly supported by the Swiss National Foundation.

References

[1] Curtins H, Wyrsch N, Favre M, and Shah A 1987 *Plasma Chem. Plasma Processing* **7** 267

[2] Howling A A, Dorier J-L, Hollenstein C, Kroll U and Finger F 1992 *J. Vac. Sci. Technol. A* **10** 1080

[3] Colgan M J, Meyyappan M, Hollenstein C, Kroll U and Murnick D E 1994 *Plasma Source Sci. Technol.* **3** 181

[4] Heintze M, Zedlitz R and Bauer G H 1993 *J. Phys. D: Appl. Phys.* **26** 1781

[5] Keppner H, Kroll U, Meyer J and Shah A 1995 *Solid State Phenomena* **44** 97

[6] Finger F, Kroll U, Viret V, Shah A, Beyer W, Tang X-M, Weber J, Howling A A and Hollenstein C 1992 *J. Appl. Phys.* **71** 5665

[7] Meiling H, Westendorp J F M, Hautala J, Saleh Z M and Malone C T 1994 *Mat. Res. Soc. Symp. Proc.* **345** 65

[8] Westendorp J F M, Meiling H, Pollock J D, Berrian D W, Laflamme A H, Hautala J and Vanderpot J 1994 *Mat. Res. Soc. Symp. Proc.* **345** 175

[9] Surendra M and Graves D B 1991 *Appl. Phys. Lett.* **59** 2091

[10] Vahedi V, Birdsall C K, Liebermann M A, DiPeso G and Rognlien T D 1993 *Phys. Fluids B* **5** 2719

[11] Schmitt J P M 1989 *Thin Solid Films* **174** 193

[12] Schmitt J P M 1992 *Mat. Res. Soc. Symp. Proc.* **219** 631

[13] Kuske J, Stephan U, Steinke O and Rhlecke S 1995 *Mat. Res. Soc. Symp. Proc.* **377** 27

[14] Okoshi T and Miyoshi T 1972 *IEEE Trans. Microwave Theory Tech.* **MTT-20** 245

[15] Sorrentino R 1985 *IEEE Trans. Microwave Theory Tech.* **MTT-33** 431

[16] Sansonnens L, Franz D, Hollenstein C, Howling A A, Schmitt J P M, Turlot E, Emeraud T, Kroll U, Meyer J and Shah A 1995 *Proc. 13th EC Photovoltaic Solar Energy Conf.* p 319

[17] Solomon I, Bhatnagar M and Rosso M 1991 *Proc. 10th EC Photovoltaic Solar Energy Conf.* p 154

[18] Forouhi A R 1989 *Properties of Amorphous Silicon* (London and New-York: INSPEC, The Inst. Electrical Engineers) p 337

[19] Morse P M and Feshbach H 1953 *Methods of Theoretical Physics* (New York: MacGraw-Hill) p 891

[20] Dorier J-L, Hollenstein C and Howling A A 1992 *J. Vac. Sci. Technol. A* **10** 1048

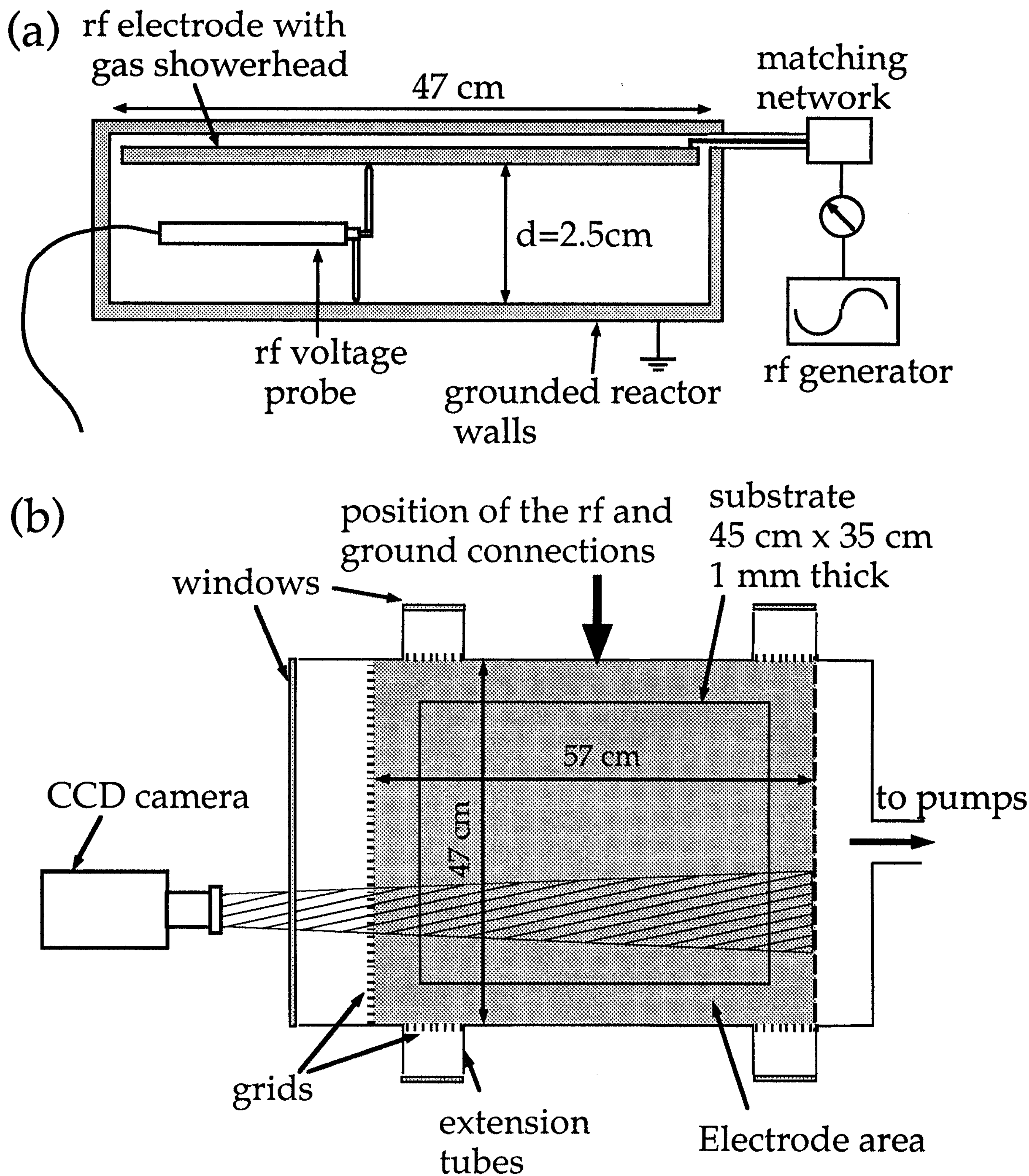

Figure 1. (a) Schematic side view of the plasma box reactor (the outer vacuum chamber is not shown) and voltage probe; (b) plan view of the reactor and substrate areas showing the windows, extension tubes and metal grids.

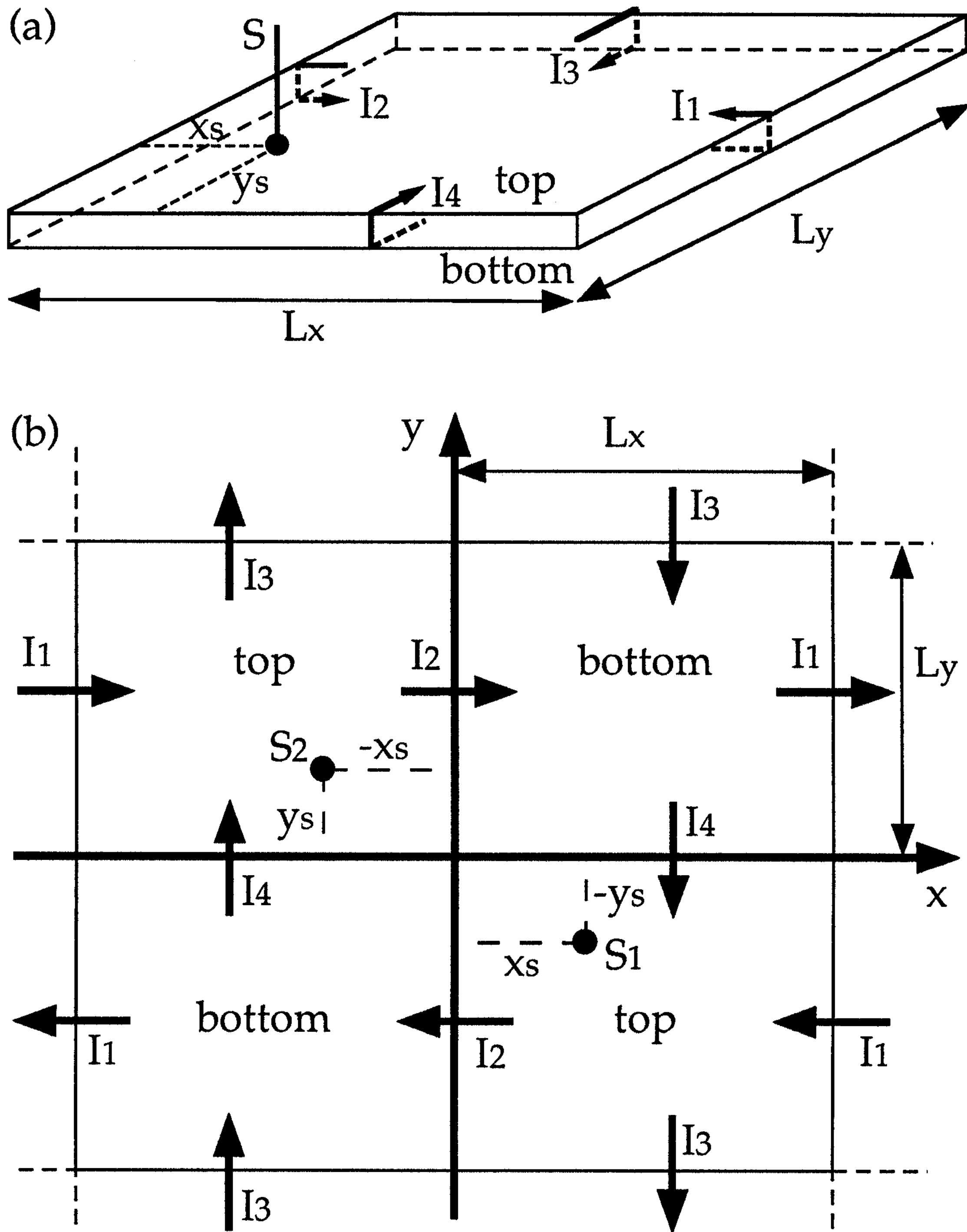

Figure 2. Schematic view of the RF electrode showing (a) the continuity of surface current flow and (b) an elementary cell in the unfolded two-dimensional geometry representation.

(a) Sources for the top voltage calculation:

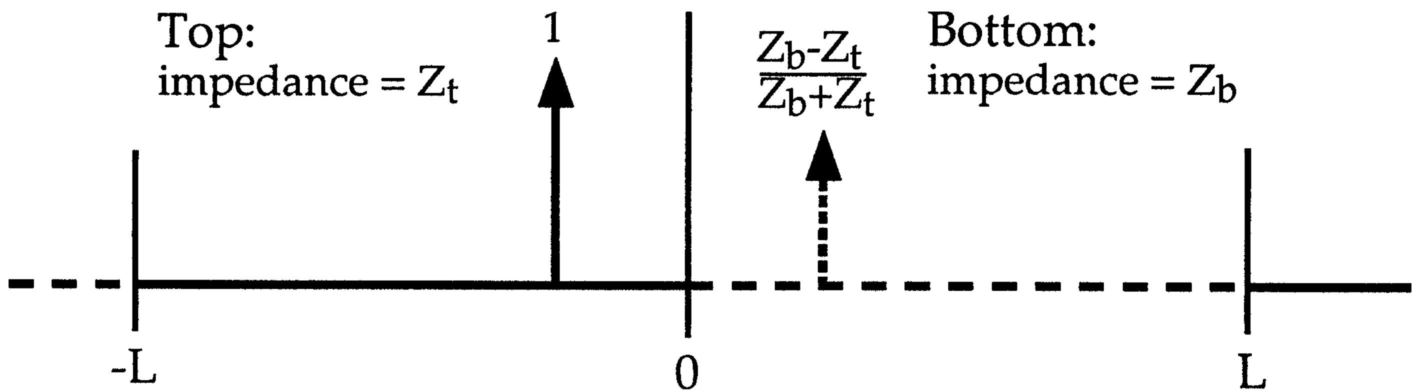

(b) Source for the bottom voltage calculation:

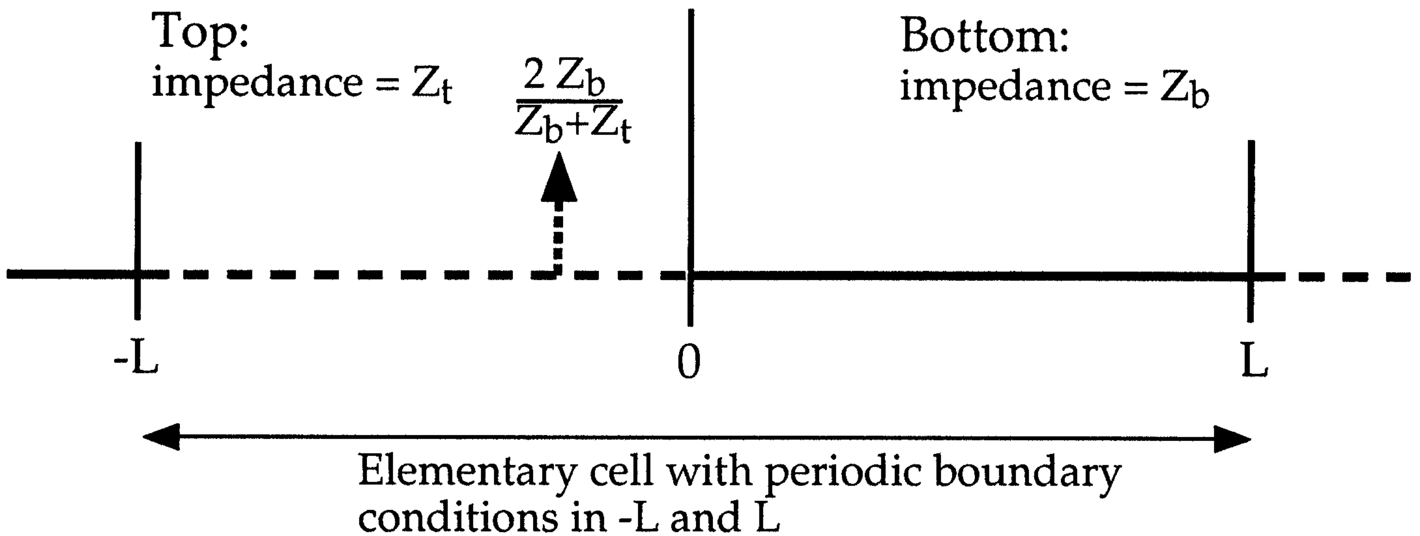

Figure 3. Schematic one-dimensional representation of the image source for the calculation of the (a) top and (b) bottom voltage distribution across the RF electrode in the case where the top and bottom characteristic impedances are different.

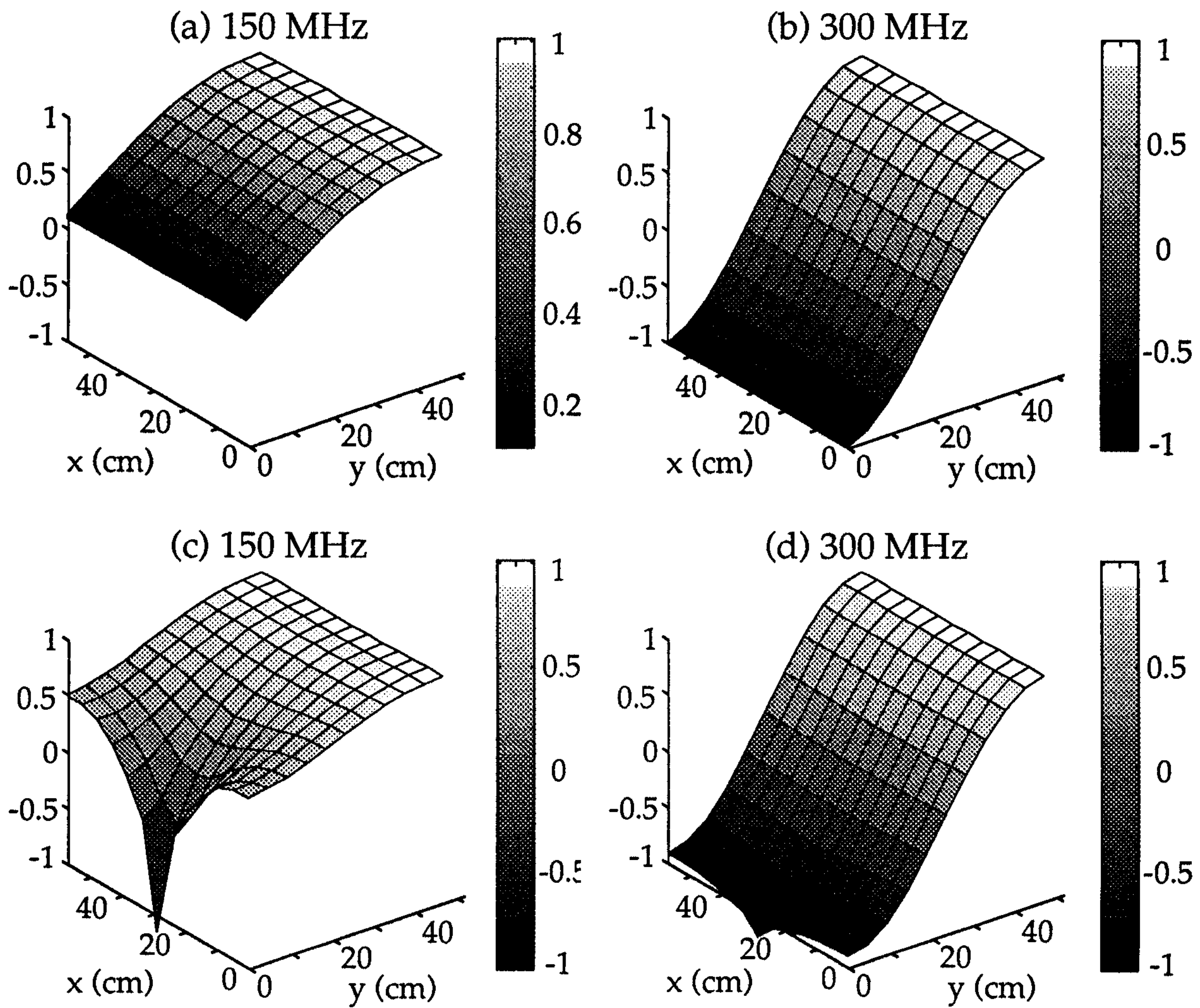

Figure 4. Normalized voltage distribution for two different frequencies: f = 150 MHz [cases (a) and (c)] and 300 MHz [(b) and (d)]. The source distribution $s = \delta(x)$ is taken to be uniform along the $x = 0$ axis for cases (a) and (b), but is point-like $s = \delta(x)\,\delta(y - L_y/2)$ for cases (c) and (d). The electrode size is 47 cm x 57 cm.

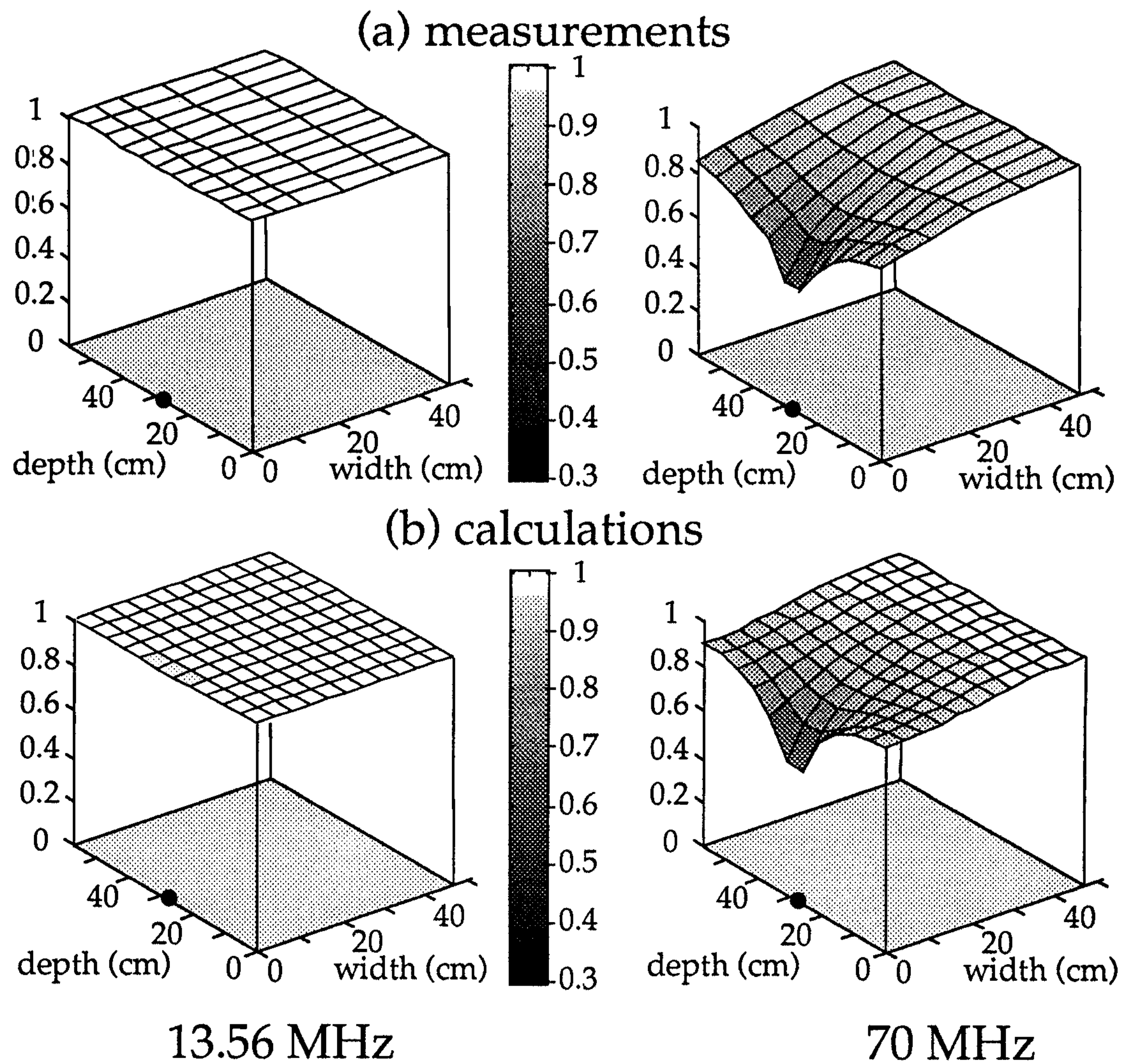

Figure 5. (a) Normalized measurements and (b) calculations of the interelectrode voltage distribution over the electrode area in absence of plasma for 13.56 MHz and 70 MHz frequencies. The black point indicates the position of the RF and ground connections.

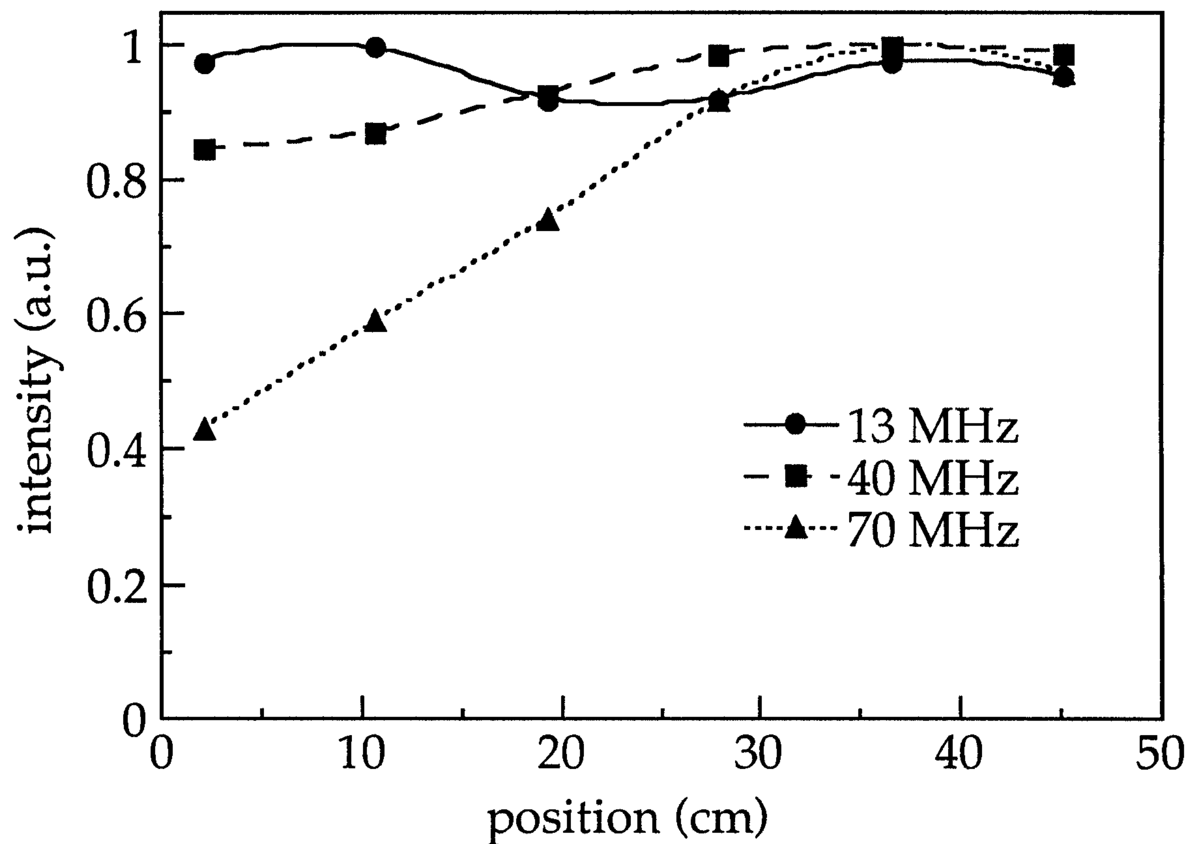

Figure 6. Emission intensity profile of an argon plasma (55 W RF power, 0.1 Torr pressure) across the front full width window for three frequencies. The intensity is integrated across the electrode gap and normalized to the maximum intensity. The position 0 cm corresponds to the side of the reactor where the RF is connected.

(a) 13.56 MHz

(b) 70 MHz

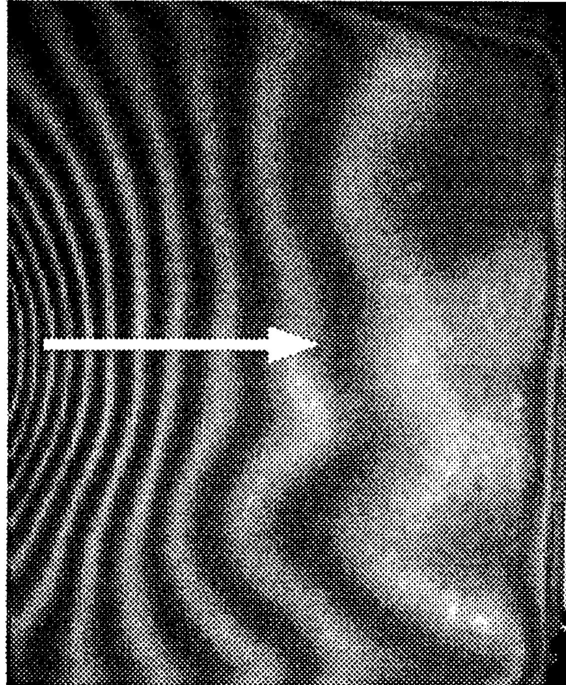

Figure 7. Global interferograms for two a-Si:H films deposited at (a) 13.56 MHz and (b) 70 MHz. The arrow shows the direction of increasing thickness.

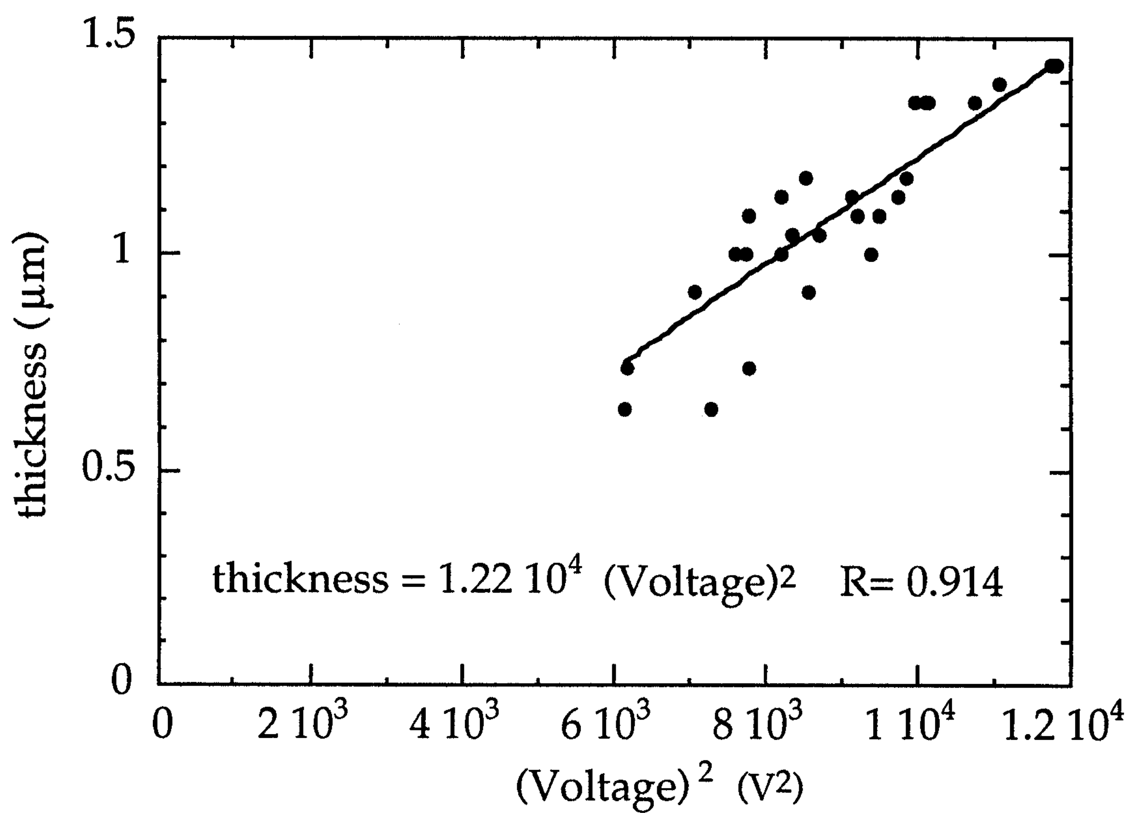

Figure 8. Dependence of the film thickness at 70 MHz on the square of the measured voltage.

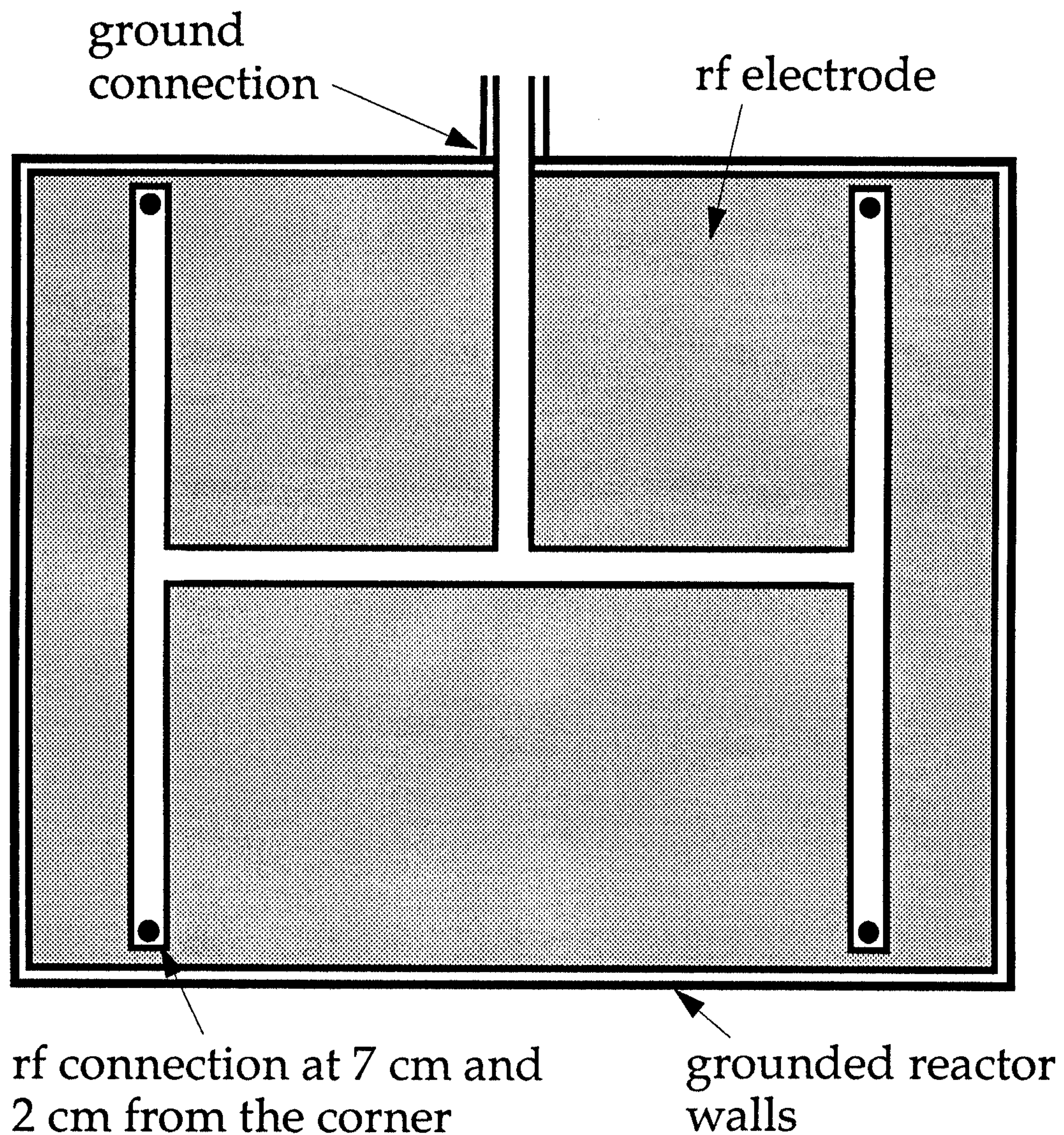

Figure 9. Schematic of the modified connection to the RF electrode. The RF connections (represented by four points) are near to the corners, and the ground connection remains midway along the longer side of the reactor. The H structure for the RF distribution assures an electrically-equivalent path for the four RF connections.

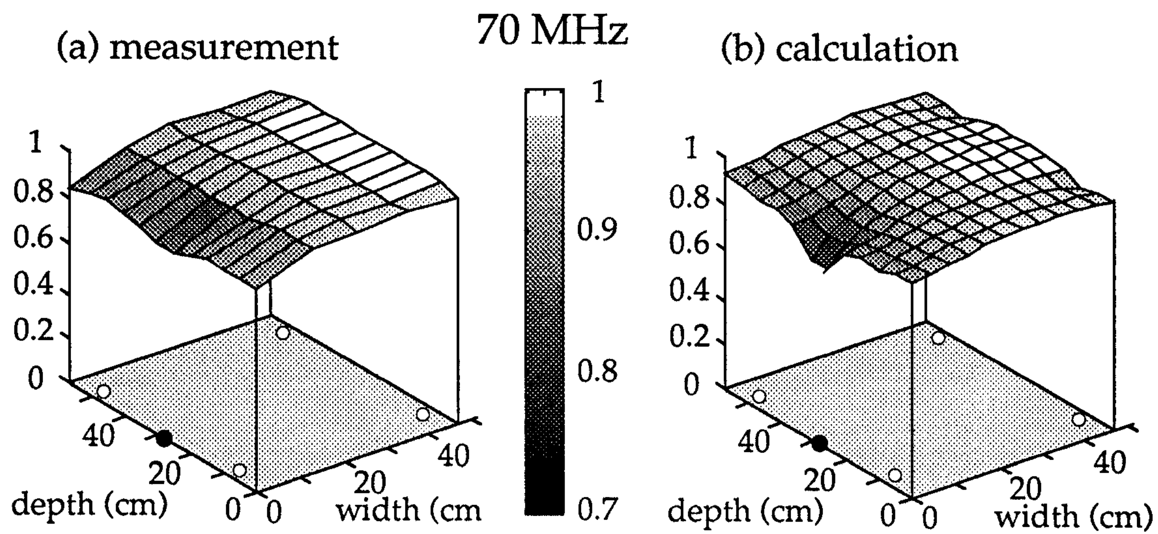

Figure 10. (a) Normalized measurement and (b) calculation of the interelectrode voltage distribution over the electrode area in the modified reactor in absence of plasma for 70 MHz frequency. The white points correspond to the RF connection positions and the black point to the ground connection.

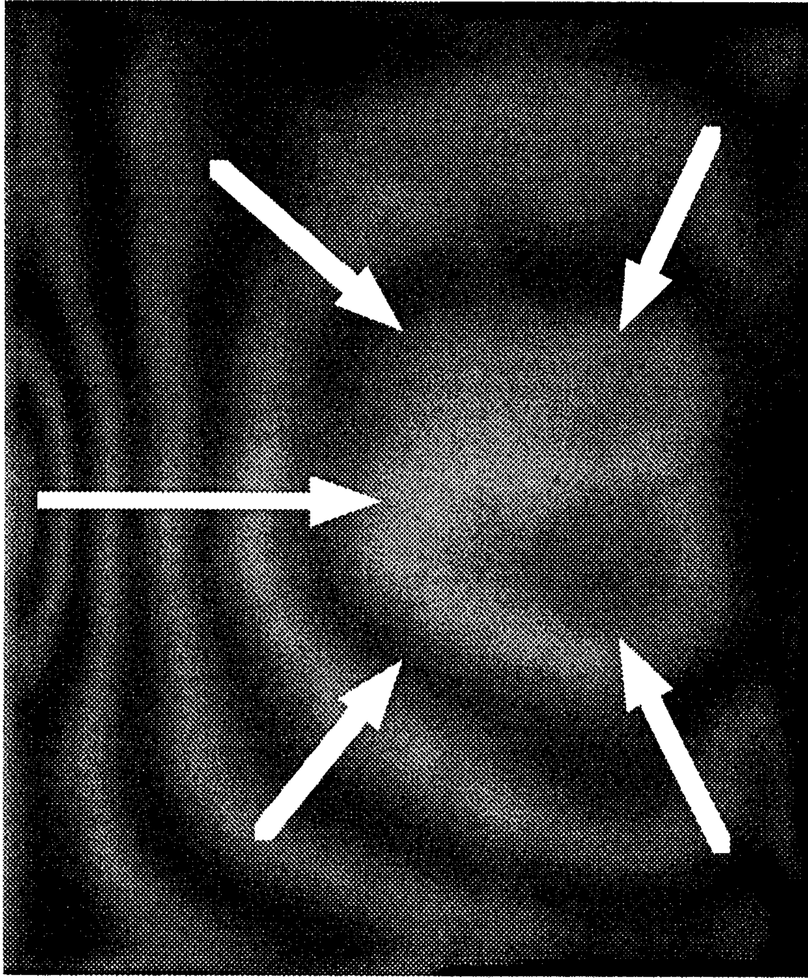

Figure 11. Global interferogram for an a-Si:H film deposited at 70 MHz using the modified RF electrode. The arrows show the direction of increasing thickness.

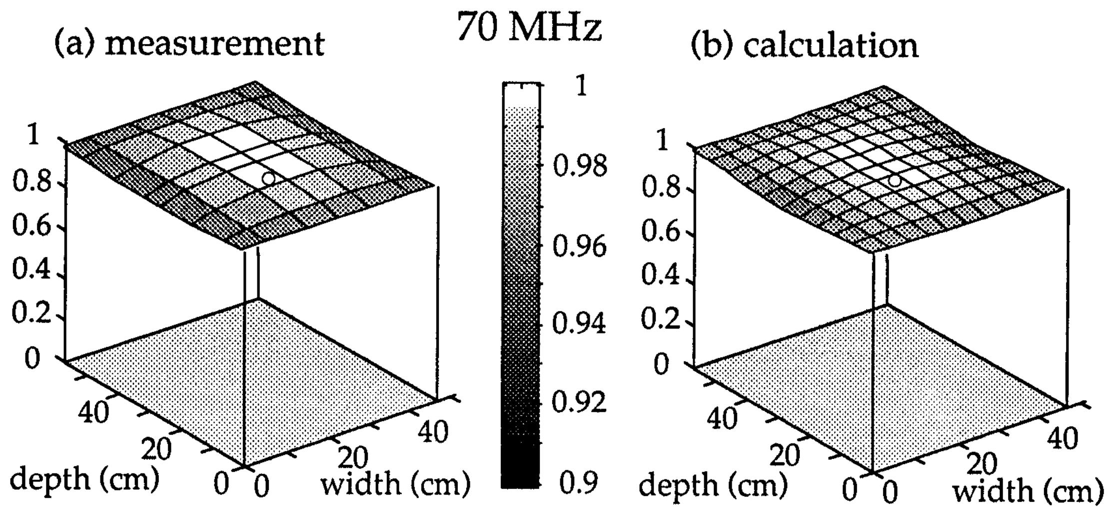

Figure 12. (a) Normalized measurement and (b) calculation of the interelectrode voltage distribution over the electrode area in absence of plasma for one RF and one ground connections centred on the top of the RF electrode and reactor cover respectively for 70 MHz frequency. The white points correspond to the RF and ground connection positions.

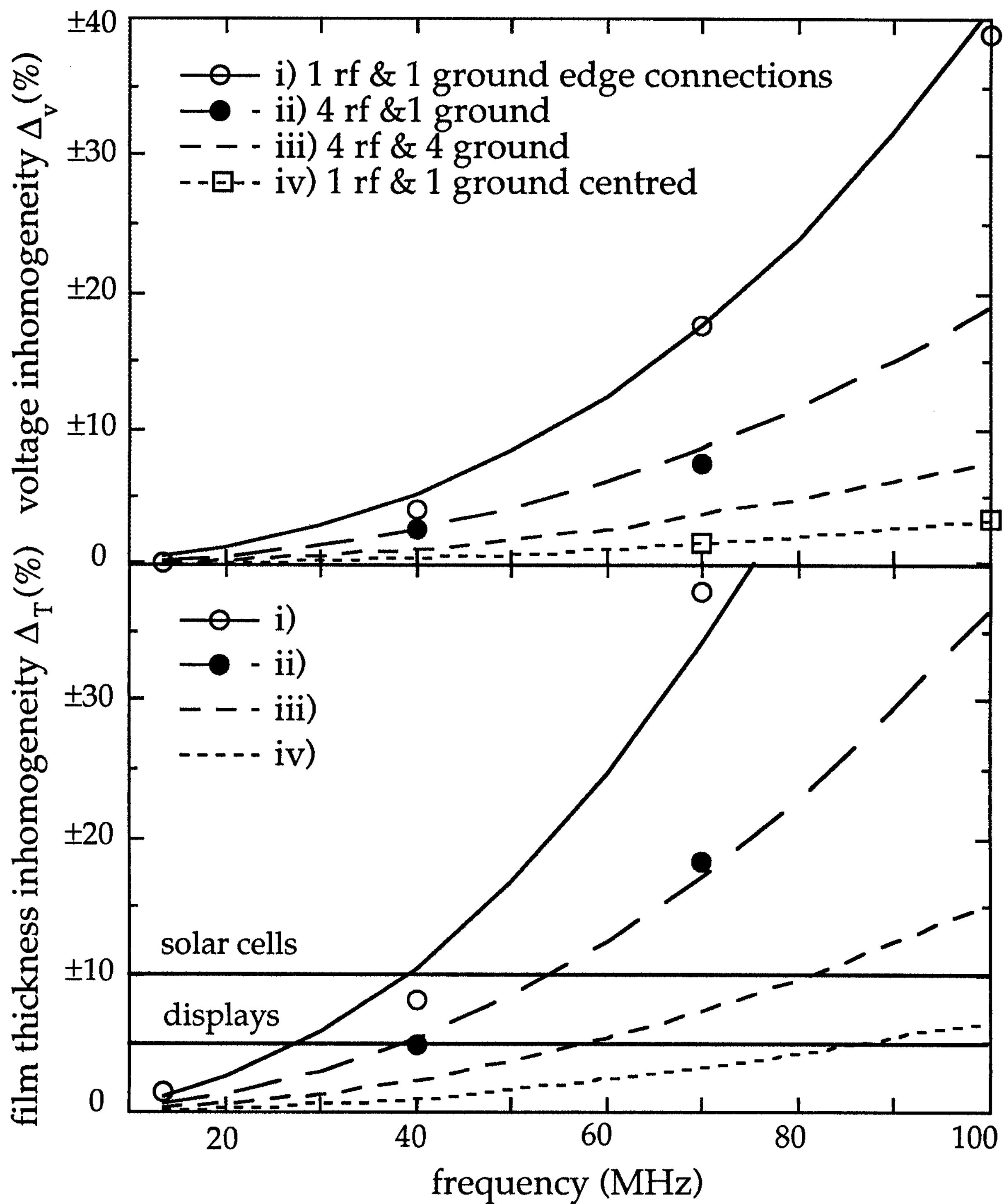

Figure 13. Dependence on the RF frequency of (a) the voltage inhomogeneity δ_V and (b) the film thickness inhomogeneity δ_T, both evaluated for the substrate area. The lines correspond to calculated values and the points to the experimental measurements. The configurations are: i) one RF and one ground connection midway along the long side of the reactor (§ 4.1); ii) four RF connections near the corners of the electrode and one ground connection midway along the long side of the reactor (§ 4.2); iii) four RF and four ground connections near the corners of the electrode (at the same location as in ii)); iv) one RF and one ground connection centred on the top of the RF electrode and reactor (§ 4.3).